RNA Conformations

DOI: 10.1002/anie.200705675

Sculpting an RNA Conformational Energy Landscape by a Methyl Group Modification—A Single-Molecule FRET Study**

*Andrei Yu. Kobitski, Martin Hengesbach, Mark Helm, and G. Ulrich Nienhaus**

RNA is a versatile biopolymer involved in a variety of key biological functions, including the storage and transport of information, structural scaffolding, and gene expression and regulation. Like proteins, RNA molecules fold into compact three-dimensional structures, and their self-assembly and dynamics are described by transitions within a highly complex energy landscape containing a vast number of different conformations. RNA forms locally stable structural motifs that assemble into larger, three-dimensional structures through tertiary interactions.[1–3] The restricted set of functional groups is frequently enriched by post-transcriptional chemical modifications of ribonucleotides, which may introduce steric conflicts and/or electrical charges or alter hydrogen-bonding patterns and π-stacking interactions.[4] Consequently, the conformational energy landscape can be sculpted so that a functionally competent fold of an RNA molecule can be selectively stabilized. A particular case in point is human mitochondrial (mt) lysine transfer RNA ($tRNA^{Lys}$), which carries a total of six modified bases.[5] One of these modifications, the methylation on N1 of adenosine 9 (m^1A9), is known to strongly affect the equilibrium between a nonfunctional, extended hairpin structure and the functional cloverleaf form (Figure 1).[6–8] Here we have studied the effect of this biologically important modification on the structure and energetics of mt $tRNA^{Lys}$ by using single-molecule fluorescence (or Förster) resonance energy transfer (smFRET), a technique that is exquisitely sensitive to structural changes on the atomic scale and allows us to distinguish different, thermally accessible conformations within the ensemble.[9–11]

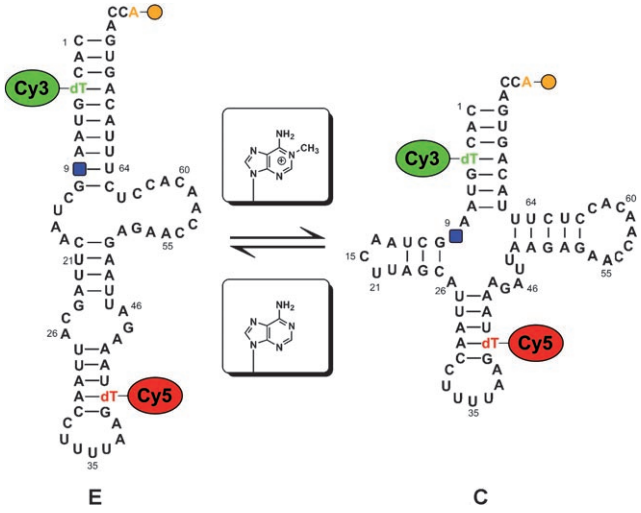

Figure 1. Secondary structures of human mt $tRNA^{Lys}$. The equilibrium between the extended hairpin (**E**) and cloverleaf (**C**) structures is markedly affected by the methylation status of adenosine 9 (blue square). The attachment sites of the Cy3 and Cy5 dyes (by means of a flexible linker at the C5 atoms of deoxythymidine) are marked in green and red, respectively; the yellow spot denotes a biotin attached for surface immobilization.[8]

Two FRET-labeled precursors of mt $tRNA^{Lys}$, the unmodified (wild-type) RNA corresponding to the genomic sequence (Kwt) and an m^1A9-modified construct (Km^1A), were synthesized.[8] By using a confocal microscope with single-molecule sensitivity,[12] we measured the FRET efficiency of these constructs by ratiometric analysis of the intensities emitted by the donor (Cy3) and acceptor (Cy5) dyes while the molecules diffused through the confocal spot of the microscope. During their brief sojourn in the sensitive volume, the excitation light was periodically switched between a green and a red laser, which allowed us to select only those molecules that carried a functional FRET pair.[13,14] Several thousand fluorescence bursts were registered and compiled in FRET efficiency histograms by grouping molecules in FRET intervals of 0.04. These measurements were performed at 16 different Mg^{2+} concentrations ranging from 0.0125 to 400 mM, as divalent ions are generally known to effectively stabilize the tertiary fold of RNA molecules, and Mg^{2+} ions are physiologically of particular relevance.[2,9,10,15–17] Variation of the Mg^{2+} concentration changes the free energies of different RNA conformations, and the energetics of Mg^{2+}–RNA interactions can be revealed by measuring the fractional populations of the RNA conformations using smFRET.[12,18] Here we have used this approach to analyze the thermodynamic effects of the m^1A9 modification in $tRNA^{Lys}$.

[*] Dr. A. Y. Kobitski, Prof. Dr. G. U. Nienhaus
Institute of Biophysics, University of Ulm
89069 Ulm (Germany)
Fax: (+49) 731-502-3059
E-mail: uli@uiuc.edu
Homepage: http://www.uni-ulm.de/nawi/nawi-biophys.html
M. Hengesbach, Dr. M. Helm
Institute of Pharmacy and Molecular Biotechnology
University of Heidelberg
69120 Heidelberg (Germany)
Prof. Dr. G. U. Nienhaus
Department of Physics
University of Illinois at Urbana-Champaign
Urbana, IL 61801 (USA)

[**] This work was supported by the Deutsche Forschungsgemeinschaft (HE 3397/3), Volkswagen Foundation, and Fonds der Chemischen Industrie.

Supporting information for this article is available on the WWW under http://www.angewandte.org or from the author.

Six select FRET efficiency histograms of Kwt and Km[1]A are shown in Figure 2. The overall shapes change markedly with Mg^{2+} concentration. Yet all measured histograms can be

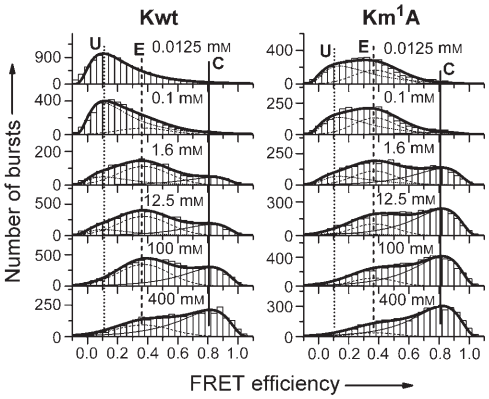

Figure 2. Histograms of FRET efficiency values measured on freely diffusing Kwt (left) and Km[1]A (right) tRNA molecules in buffer solutions at six different Mg^{2+} concentrations. Dotted, dashed, and solid thin lines represent best-fit model distributions for the **U**, **E**, and **C** states, respectively; the solid thick line gives the sum of the three distributions.

modeled as superpositions of three FRET efficiency distributions peaking at low, intermediate, and high FRET values. They represent three subpopulations, which we denote by **U** (for "unfolded"), **E** (for "extended hairpin"), and **C** (for "cloverleaf-based L-shape") for reasons that will be explained below. In the quantitative analysis, the FRET histograms were fitted with a sum of two log-normal functions for the **U** and **C** states and a normal Gaussian for the **E** state.[12,19–21] As the individual subpopulations are broad and overlapping, a global fit of all 32 histograms was performed, using identical position and width parameters for the three distributions; the best-fit parameters of these distributions are compiled in Table 1.

Table 1: Average FRET efficiency, $\langle E \rangle$, and full width at half maximum (FWHM) parameters from a global fit of a sum of three model distributions for the **U**, **E**, and **C** conformations to the measured FRET efficiency histograms of $tRNA^{Lys}$. Also included are the distances r between the dye units as calculated from $\langle E \rangle$ (see text).

	Fit function	$\langle E \rangle$	FWHM	$r(\langle E \rangle)$ [Å] calcd
U	log normal	0.25 ± 0.02	0.32 ± 0.03	81
E	normal	0.37 ± 0.01	0.41 ± 0.03	65
C	log normal	0.69 ± 0.02	0.37 ± 0.03	46

Excellent agreement was obtained between fits (lines in Figure 2) and experimental data for all Mg^{2+} concentrations, which suggests that both tRNA constructs can assume three distinct conformations **U**, **E**, and **C**, with structural properties that are sufficiently similar between the two RNA constructs that we cannot distinguish them with our technique.

FRET experiments provide structural information owing to the strong distance, r, dependence of the donor–acceptor coupling [Eq. (1)] with the Förster radius $R_0 = 53$ Å for an orientationally averaged Cy3/Cy5 dye pair in aqueous solution.[22,23]

$$E = \frac{R_0^6}{r^6 + R_0^6} \quad (1)$$

For the distribution of the **C** state, the measured $\langle E \rangle$ corresponds to $r = 46.4$ Å according to Equation (1). This value is similar to the distance between the dye attachment sites, which was found to be 42.8 Å in the crystal structure of yeast $tRNA^{Phe}$.[24] By using dye-labeled DNA constructs, we had earlier found that the Förster radius is close to the distance between the attachment points because the dyes are connected by means of linkers and fluctuate around these points.[23] Therefore, the measured FRET efficiency strongly supports the assignment of state **C** to the cloverleaf-based L-shape structure of the folded tRNA. For the **E** state, the structure is not known, but comparative solution mapping indicates that the RNA forms an extended hairpin consisting of three helices connected by two loops (Figure 1).[25] Moreover, transient electric birefringence measurements revealed an angle of $\approx 140°$ between the acceptor and anticodon stems.[5] By taking distances of 3.4 Å and 6.3 Å for nucleotides in helices and loops, respectively, and an angle of 140° between the two arms, we estimate a total distance between the dye attachment sites of ≈ 75 Å. The simple Förster relation yields a somewhat smaller distance, $r = 58$ Å for $\langle E \rangle = 0.37$. We note, however, that the **E** state may be rather flexible, so that the assumption of a fixed distance may not hold. A relation based on the Gaussian chain, which takes E as an average over all dye distances and orientations of a fluctuating chain,[12,20,26] yields $r = 65$ Å, which is still smaller than our estimate. This result may suggest that the region between the central domain and the anticodon loop is more condensed than shown in Figure 1. For state **U**, no a priori structural information is available. A completely random, Gaussian RNA chain would give an average distance of 102 Å between the dyes (see the Supporting Information), whereas $\langle E \rangle = 0.25$ of state **U** corresponds to $r = 81$ Å using the Förster relation for a fluctuating chain.[12] The smaller value implies that the RNA in state **U** still retains some residual structure.

In Figure 3 the fractional subpopulations of the **U**, **E**, and **C** states of Kwt and Km[1]A are plotted as a function of the Mg^{2+} ion concentration. For both constructs, a pronounced drop of the **U** state population is observed with increasing Mg^{2+} concentration, with a midpoint at ≈ 0.5 mM, which is accompanied by an increase of the ***C*** state population. The **E** state population, however, increases for Kwt but decreases for Km[1]A. At higher concentration (≈ 100 mM), a second transition is evident in which the **C** state increases at the expense of the **E** state for both constructs.

For a quantitative analysis of the Mg^{2+}-dependent populations in the **U**, **E**, and **C** states, we have decomposed the Mg^{2+}-induced RNA folding reaction into an RNA folding reaction and a Mg^{2+} binding reaction[10] in each of the three states, which yields the six-state thermodynamic model depicted in Figure 4. The fractional populations of the six states are governed by five independent equilibria. Three of

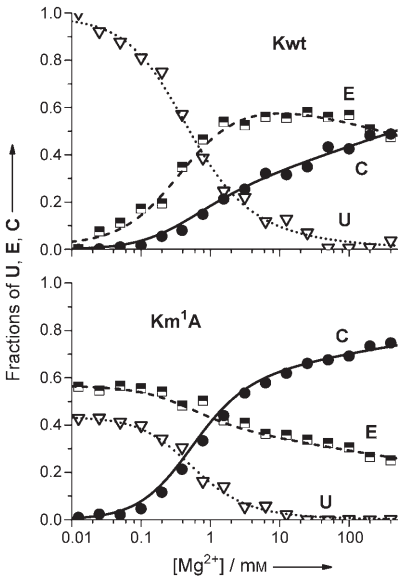

Figure 3. Mg^{2+} dependence of the fractional populations in the **U**, **E**, and **C** states. Lines represent results from fitting the data with the thermodynamic model depicted in Figure 4.

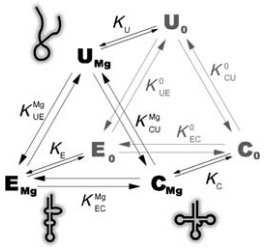

Figure 4. Thermodynamic scheme describing the equilibria between the Mg-free and Mg-bound forms of the **U**, **E**, and **C** states and their relative energies.

them involve the population ratios between the Mg-free and Mg-bound conformations within the **U**, **E**, and **C** states [Eq. (2)].

$$K_i = \frac{[i_0]}{[i_{Mg}]} \exp\left(-\frac{\Delta G_i(Mg)}{RT}\right) \quad (2)$$

Here, the brackets denote the fractional populations; K_i and ΔG_i(Mg) are the equilibrium coefficients and free energy differences between Mg-bound (subscript "Mg") and Mg-free (subscript "0") conformations within state i; and R and T represent the gas constant and the absolute temperature, respectively. We note that our FRET experiment can only distinguish states **U**, **E**, and **C**, but not the Mg-bound and Mg-free conformations within each state. Therefore, only the sums $[U_0 + U_{Mg}]$, $[E_0 + E_{Mg}]$, and $[C_0 + C_{Mg}]$ can be measured and are plotted in Figure 3. The Mg^{2+} dependence of the free energies is modeled by Equation (3).[27]

$$\Delta G_i(Mg) = \Delta G_i^\circ + n_i RT \ln[Mg^{2+}] \quad (3)$$

Here ΔG_i° represents the standard free energy of each state i. The cooperativity parameter (or Hill coefficient), n_i, quantifies the sharpness of the transition. Two more equations determine the relative populations of the three states **U**, **E**, and **C** [Eqs. (4a,b)].

$$K_{UE}^\circ = \frac{[E_0]}{[U_0]} = \exp\left(-\frac{\Delta G_{UE}^\circ}{RT}\right) \quad (4a)$$

$$K_{EC}^\circ = \frac{[C_0]}{[E_0]} = \exp\left(-\frac{\Delta G_{EC}^\circ}{RT}\right) \quad (4b)$$

Mathematical details of the thermodynamic model are provided in the Supporting Information. The lines in Figure 3 show the Mg^{2+} dependence of the **U**, **E**, and **C** populations from a nonlinear least-squares fit of this model to the data; the resulting fit parameters, ΔG_i°, n_i, and the two free energy differences ΔG_{UE}^0 and ΔG_{EC}^0 are given in Table 2 for both Kwt and Km^1A. The identical Hill coefficients (within error) of Kwt and Km^1A within the three states lend independent support to our assertion based on the FRET efficiency distributions that the **U**, **E**, and **C** states are structurally similar for Kwt and Km^1A. The Mg^{2+}-dependent populations of the six thermodynamic states are shown in the Supporting Information.

Table 2: Cooperativity parameters and free energies as determined from the thermodynamic model.

Fit parameter	Kwt	Km^1A
n_U	0.7 ± 0.1	0.7 ± 0.1
n_E	1.06 ± 0.03	1.10 ± 0.04
n_C	1.21 ± 0.03	1.20 ± 0.04
ΔG_U°) kJ mol^{-1}	10.8 ± 1.2	8.9 ± 2.8
ΔG_E°) kJ mol^{-1}	29.9 ± 0.3	24.0 ± 0.2
ΔG_C°) kJ mol^{-1}	47.2 ± 0.3	47.2 ± 0.2
ΔG_{UE}°) kJ mol^{-1}	9.9 ± 0.4	-0.7 ± 0.3
ΔG_{EC}°) kJ mol^{-1}	16.9 ± 0.3	24.0 ± 0.2

The free energies of the Mg-free and Mg-bound (at 1M) states are represented in Figure 5; the U_0 states of both constructs were set to 0. Two major differences between Kwt and Km^1A are clearly evident: in Km^1A, state E_0 is ≈ 10 kJ mol^{-1} and both C_0 and C_{Mg} are ≈ 3 kJ mol^{-1} lower in free energy than in Kwt. Note that the stabilization of E_0 in Km^1A is clearly obvious from its large population at low Mg^{2+} concentrations (Figure 3). The transition from U_0 to E_0 and hence the compactization of Kwt in the Mg-free form increases its free energy as a result of electrostatic repulsion. By contrast, a slight decrease is observed for Km^1A, which is likely owing to electrostatic stabilization of E_0 by the positive charge on the methylated A9. For the Mg-bound form E_{Mg} of Km^1A, the stabilizing effect is much smaller, however. Possibly, Mg^{2+} binding to the **E** state interferes with favorable hydrogen bonding of m^1A9, for example, in the base pair m^1A9–U64. In the **C** state, the stabilizing effect of the positive charge is also comparatively small, which may indicate that the base of nucleotide m^1A9 does not participate in base-pair

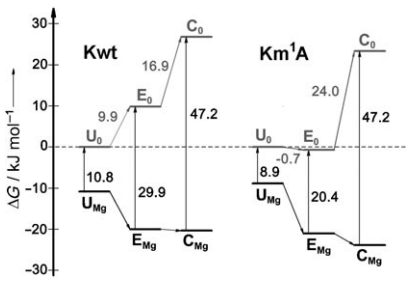

Figure 5. Free energy diagram of the populations $\mathbf{U}_0$, $\mathbf{E}_0$, and $\mathbf{C}_0$ of Mg^{2+}-free, and $\mathbf{U}_{Mg}$, $\mathbf{E}_{Mg}$, and $\mathbf{C}_{Mg}$ (at 1 M Mg^{2+}) of Mg^{2+}-bound Kwt and Km^1A $tRNA^{Lys}$ resulting from fits with the model in Figure 4.

stabilization of the cloverleaf structure and is likely exposed to the solvent.[28]

We have explored Mg^{2+}–RNA interactions and conformational equilibria among three distinct conformations of human mt $tRNA^{Lys}$. By extending the smFRET technique to the study of RNAs containing modified nucleotides, we could quantitatively assess the effect of a single methyl group on the conformational equilibria. All three main conformations are significantly populated at physiological Mg^{2+} concentration, whereas previous chemical probing studies suggested that the m^1A9 modification switches the tRNA from the extended form **E** to the cloverleaf form **C**.[6] This difference may result from the fact that, unlike chemical probing, smFRET experiments are performed under conditions of strict thermal equilibrium. In the near future, we will extend our work to other naturally occurring tRNA modifications, including the five remaining ones in $tRNA^{Lys}$.[4] Our approach may also be easily applicable to various RNA (or DNA) structure–function studies involving nonnatural nucleotide modifications, which are often referred to as "atomic mutagenesis".

Experimental Section

FRET-labeled Kwt and K^1mA were prepared as described.[8] Briefly, an RNA fragment containing the m^1A9 modification was synthesized by solid-phase phosporamidite chemistry employing a 1-methyladenosine phosphoramidite and a modified deprotection protocol.[25] Other RNA fragments were purchased (IBA, Göttingen, Germany). Cy3 and Cy5 were introduced into separate oligoribonucleotides by postsynthetic NHS coupling to amino-linker-carrying deoxythymidine nucleotides corresponding to positions 4 and 41, respectively, in the full-length tRNA.[8] Finally, the tRNA constructs were assembled from the RNA fragments by splint ligation.[29]

Solutions of tRNA ($\approx$100 pM) and various Mg^{2+} concentrations were prepared by mixing distilled water (Fluka, Taufkirchen, Germany), 50 mM Tris-HCl buffer, pH 7.4, 1M $MgCl_2$, and tRNA solutions in the appropriate proportions. The tRNA solutions were heated to 60 °C for 3 min and then slowly cooled to room temperature prior to the measurements. For smFRET experiments, the samples were kept between two cover slips as described.[9]

Single-molecule fluorescence measurements were performed on a home-built laser scanning confocal microscope with two-channel detection.[12,30] Laser excitation was alternated every 100 µs between the green 514.5 nm line of an Ar^+/Kr^+ ion laser (modified model 164, Spectra-Physics, Mountain View, CA) for Cy3 and the red 633 nm line of a He–Ne laser for Cy5 by passing the laser beams through an acousto-optical tunable filter (AOTF, AA Opto-Electronic, Orsay, France). The fluorescence emission was collected by a water-immersion objective (UPlan-Apo 60×/1.20w, Olympus, Hamburg, Germany), passed through a pinhole 100 µm in diameter, separated into donor (555–610 nm) and acceptor (650–750 nm) channels by using a beam splitter at 640 nm (HQ640DCXR, AHF, Tübingen, Germany) and filters optimized for donor (HQ582/50, AHF) and acceptor (emitter Cy3/Cy5, AHF) emission, and finally detected with avalanche photodiodes (SPCM-CD 3017, PerkinElmer, Boston, MA, USA). Photon counts were registered in the computer with 10 µs bin time using a multifunctional data acquisition card (NI PCI-6229, National Instruments, München, Germany). Details of the data analysis are given in the Supporting Information.

Received: December 11, 2007
Published online: April 30, 2008

Keywords: conformation analysis · FRET (fluorescence resonance energy transfer) · RNA · single-molecule studies · thermodynamic analysis

[1] D. Thirumalai, C. Hyeon, *Biochemistry* **2005**, *44*, 4957–4970.
[2] P. Brion, E. Westhof, *Annu. Rev. Biophys. Biomol. Struct.* **1997**, *26*, 113–137.
[3] J. N. Onuchic, Z. Luthey-Schulten, P. G. Wolynes, *Annu. Rev. Phys. Chem.* **1997**, *48*, 545–600.
[4] M. Helm, *Nucleic Acids Res.* **2006**, *34*, 721–733.
[5] M. A. Leehey, C. A. Squassoni, M. W. Friederich, J. B. Mills, P. J. Hagerman, *Biochemistry* **1995**, *34*, 16235–16239.
[6] M. Helm, R. Giegé, C. Florentz, *Biochemistry* **1999**, *38*, 13338–13346.
[7] M. Helm, G. Attardi, *J. Mol. Biol.* **2004**, *337*, 545–560.
[8] F. Voigts-Hoffmann, M. Hengesbach, A. Y. Kobitski, A. van Aerschot, P. Herdewijn, G. U. Nienhaus, M. Helm, *J. Am. Chem. Soc.* **2007**, *129*, 13382–13383.
[9] H. D. Kim, G. U. Nienhaus, T. Ha, J. W. Orr, J. R. Williamson, S. Chu, *Proc. Natl. Acad. Sci. USA* **2002**, *99*, 4284–4289.
[10] V. K. Misra, D. E. Draper, *J. Mol. Biol.* **2002**, *317*, 507–521.
[11] G. U. Nienhaus, *Macromol. Biosci.* **2006**, *6*, 907–922.
[12] A. Y. Kobitski, A. Nierth, M. Helm, A. Jäschke, G. U. Nienhaus, *Nucleic Acids Res.* **2007**, *35*, 2047–2059.
[13] A. N. Kapanidis, N. K. Lee, T. A. Laurence, S. Doose, E. Margeat, S. Weiss, *Proc. Natl. Acad. Sci. USA* **2004**, *101*, 8936–8941.
[14] B. K. Müller, E. Zaychikov, C. Bräuchle, D. C. Lamb, *Biophys. J.* **2005**, *89*, 3508–3522.
[15] X. W. Fang, T. Pan, T. R. Sosnick, *Nat. Struct. Biol.* **1999**, *6*, 1091–1095.
[16] R. Russell, X. Zhuang, H. P. Babcock, I. S. Millett, S. Doniach, S. Chu, D. Herschlag, *Proc. Natl. Acad. Sci. USA* **2002**, *99*, 155–160.
[17] G. Bokinsky, D. Rueda, V. K. Misra, M. M. Rhodes, A. Gordus, H. P. Babcock, N. G. Walter, X. Zhuang, *Proc. Natl. Acad. Sci. USA* **2003**, *100*, 9302–9307.
[18] D. Grilley, A. M. Soto, D. E. Draper, *Proc. Natl. Acad. Sci. USA* **2006**, *103*, 14003–14008.
[19] B. Schuler, E. A. Lipman, W. A. Eaton, *Nature* **2002**, *419*, 743–747.
[20] E. V. Kuzmenkina, C. D. Heyes, G. U. Nienhaus, *J. Mol. Biol.* **2006**, *357*, 313–324.
[21] E. V. Kuzmenkina, C. D. Heyes, G. U. Nienhaus, *Proc. Natl. Acad. Sci. USA* **2005**, *102*, 15471–15476.
[22] Y. Ishii, T. Yoshida, T. Funatsu, T. Wazawa, T. Yanagida, *Chem. Phys.* **1999**, *247*, 163–173.
[23] O. Coban, D. C. Lamb, E. Zaychikov, H. Heumann, G. U. Nienhaus, *Biophys. J.* **2006**, *90*, 4605–4617.

[24] H. Shi, P. B. Moore, *RNA* **2000**, *6*, 1091 – 1105.
[25] M. Helm, H. Brulé, F. Degoul, C. Cepanec, J. P. Leroux, R. Giegé, C. Florentz, *Nucleic Acids Res.* **1998**, *26*, 1636 – 1643.
[26] B. Schuler, *ChemPhysChem* **2005**, *6*, 1206 – 1220.
[27] D. E. Draper, D. Grilley, A. M. Soto, *Annu. Rev. Biophys. Biomol. Struct.* **2005**, *34*, 221 – 243.
[28] P. F. Agris, H. Sierzputowska-Gracz, C. Smith, *Biochemistry* **1986**, *25*, 5126 – 5131.
[29] W. C. Kurschat, J. Müller, R. Wombacher, M. Helm, *RNA* **2005**, *11*, 1909 – 1914.
[30] E. V. Amirgoulova, J. Groll, C. D. Heyes, T. Ameringer, C. Röcker, M. Möller, G. U. Nienhaus, *ChemPhysChem* **2004**, *5*, 552 – 555.

